Gibbs ensemble simulation of water in spherical cavities

Ivan Brovchenko, Dietmar Paschek, and Alfons Geiger[a)]
Physikalishe Chemie, Universitat Dortmund, 44221 Dortmund, Germany

(Received 8 February 2000; accepted 26 June 2000)

Chemical equilibration with a bulk reservoir is the crucial problem in computer simulations of liquids in confined geometries. The Gibbs ensemble simulation method is used in the present paper to solve this problem for water in pores. MC simulations of TIP4P water in spherical cavities with smooth surfaces and radii from 6 to 15 Å were done in equilibrium with bulk water at $T=300$ and 350 K. Chemical equilibration between confined and bulk water was obtained by an essential number of molecular transfers. To our knowledge this is the first application of the Gibbs ensemble simulation method for the equilibration of two dense liquid water systems. As most important result we find that liquid water exists in a cavity only if the water–substrate interaction exceeds some critical value. An increase of the average water density by about 20% with the strengthening of the interaction is observed. For all systems there are two prominent water layers near the cavity surface which exhibit strong orientational ordering. The pair correlation functions evidence a strong distortion of the tetrahedral water structure in the first, outer layer towards a square lattice arrangement. The diffusivity of the water in the cavity always decreases with respect to the bulk. [S0021-9606(00)50336-5]

I. INTRODUCTION

The investigation of water which is confined in different environments is of great importance for the understanding of many technological and biophysical processes. Its structural and dynamical properties differ essentially from the bulk. This is caused by both the geometrical confinement and its interaction with the interface.

The behavior of water confined in pores was the subject of numerous experimental and theoretical studies. Freezing experiments show the existence of two kinds of water in pores: ''free'' water in the center of the pore and ''bound'' water near the pore surface.[1–12] The shift of the freezing temperature of the ''free'' water achieves −60 K (Ref. 11) and is roughly inversely proportional to the pore radius in accordance with Kelvin's equation.[4,5,8,11] On freezing, ''free'' water transforms into cubic ice[1–3,8–11,13] and its stability with respect to the ordinary hexagonal ice increases as the pore becomes smaller.[3] For the ''bound'' water the phase transition is smeared out and its temperature range (180–220 K) does not depend on the pore size.[6,8,11] Estimations of the thickness of the ''bound'' water layer by different experimental methods[3,4,6–8,11,12,14,15] yield 1–3 water monolayers. In pores with a radius of less than approximately 10–12 Å only ''bound'' water remains and there is no sharp solid–liquid phase transition in such small pores.[6,8,11,16,17] X-ray diffraction experiments show that the ''bound'' water possesses little short-range order.[3]

The diffusivity of water decreases in confined environments with respect to the bulk behavior.[18–23] This effect strengthens with decreasing pore size.[19,20] Slowing-down of the water diffusivity by an order of magnitude was observed.[19,20,21] Experimental investigations of water adsorption in pores with different ratios of hydrophilic and hydrophobic groups on the wall show, that liquid water stops penetrating the pore sharply at some level of hydrophobicity.[5]

Numerous molecular dynamics (MD) and Monte Carlo (MC) simulations of water in slitlike,[24–54] cylindrical,[55–60] and spherical[61–66] pores were reported. Smooth and structured substrates with different strengths of water–substrate interactions were considered. For strong water–substrate interaction (metallic and polar substrates) the variation of the water density along the distance from the surface shows strong layering with a few distinct layers and a local density maximum in the outer water layer exceeding 2.0 g/cm^3.[27,29,33–36,38–40,42,43,45,47,48,50–56,59] Water near a weak-interacting substrate[24–26,28,30–32,37,41,42,44,46,49–51,57,58] or near a free surface[59,67,68] shows weak layering without essential density variations. In all cases water molecules show orientational ordering near the interface with a tendency to keep the orientation of the dipole moment parallel to the surface in order to maximize the number of water–water hydrogen bonds. When calculating the water self-diffusion coefficient in pores, both decrease[37,42,47,52,56,60] and increase[25–27,31,42,58,64] of water diffusivity with respect to its bulk behavior were obtained.

The degree of water layering near the surface, its orientational ordering and molecular mobility depend on the strength of the water–substrate interaction, details of the substrate structure, and on the average water density in the pore. The more or less arbitrary choice of the number of water molecules in the pores is one of the main sources of the observed discrepancies. The necessity to provide a correct chemical equilibration of the pore water with a bulk reservoir was emphasized by many authors.[33,43,44,51,58,60]

Circumventing this equilibration, in most of the above mentioned simulations the water density in the pore was fixed at approximately the bulk density. However, a simple

a)Author to whom correspondence should be addressed.

adjustment of the average water density to the bulk value[24–30,32,33,37,46,50,56,57,61,64,65] does not mean that confined water is in equilibrium with the bulk. This is clearly seen in simulations of liquids in pores with different water–substrate interactions. Strengthening of this interaction results in an adsorption of the liquid on the pore walls, whereas the pore center becomes empty. An adjustment of the liquid density in the center of the pore to its bulk value[31,39,41,49,52–54,58,60,62,63] could not solve this problem. Such an approach assumes that the amount of the liquid in the center of the pore, which is not disturbed by confinement and interactions with the surface, is sufficient to reproduce the bulk behavior. This may be correct for large slitlike pores, but it is obviously not correct for nanopores and especially pores of cylindrical or spherical geometry.

A natural way to obtain systems in chemical equilibrium are simulations in the grand canonical ensemble (GCE) (Ref. 69) or Gibbs ensemble (GE).[70,71] They were widely used for the simulation of simple model liquids in pores of different types [GCE (Refs. 72–75) and GE (Refs. 71, 76–78)]. The main problems in such simulations are connected with the necessity to provide an essential number of molecular insertions (deletions) into (from) the dense liquid phase. These problems grow sharply for such dense and associated liquids as water. In view of these difficulties most of the simulations of water in pores were done without chemical equilibration with the bulk and with a rather arbitrary choice of the water density in the pores.

To avoid molecular transfers, some indirect and approximative techniques were used: simulation in the isotension ensemble,[44] use of a linear superposition approximation for the density,[43] simulation of a pore and bulk water in one box.[51] In all these cases questions remain about the validity of these approaches for liquid water and about the quality of the chemical equilibration.

There are only a few simulations of water in pores using the grand canonical ensemble with the bulk value of the chemical potential.[35,36,38,47,55] The quality of the chemical equilibration with the bulk in such an approach depends both on the accuracy of the computation of the chemical potential of the bulk water and on the equilibration of the pore water. The latter factor is determined mainly by the number of successful insertion and deletion of molecules. With the additional problems of the accurate calculation of the chemical potential of liquid water,[79,80] the possibility to avoid such calculations in a Gibbs ensemble simulation is attractive.

A Gibbs ensemble simulation of confined water in equilibrium with water vapor was reported,[45,81] but there are no such simulations in equilibrium with liquid water. These kinds of simulations provide the most direct and accurate way for equilibration of confined and bulk water by an essential number of molecular transfers between the two phases. As mechanical equilibrium has not to be established explicitly in such systems,[71] the bulk water may be kept at constant pressure and temperature, and simultaneously the pore water at the same temperature and constant pore volume. There is a close resemblance to grand canonical ensemble simulation, but instead of specifying a common value of the chemical potential for both systems, the simulation box with the bulk water is used for chemical equilibration directly. This procedure yields a higher accuracy of the simulation by speeding up the equilibration process. This is the main reason of our decision to use Gibbs ensemble simulation in the present paper.

In the present paper water in spherical cavities in equilibrium with a bulk reservoir was simulated in the Gibbs ensemble. The dependence of the structural and dynamical water properties on water–substrate interaction, cavity size, and temperature is analyzed.

II. SIMULATION METHOD

512 TIP4P water molecules in a cubic box with periodic boundary conditions were used to reproduce bulk water at $P=1$ bar and $T=300$ K, respectively 350 K. Intermolecular interactions were calculated up to a cutoff distance of 12 Å and long-range corrections were included for the Lennard-Jones potentials only. Spherical cavities with radii R_c from 6 to 15 Å were considered. The water–water interactions in the cavity were calculated without cutoff. The water–substrate interaction was simulated as a Lennard-Jones (9-3) potential

$$U_{w-s}(r)=\epsilon[(\sigma/r)^9-(\sigma/r)^3],$$

where r is the distance between the oxygens and the substrate. The parameter σ in this potential was fixed to 2.5 Å, the parameter ϵ varied to change the well-depth $U=-0.385\epsilon$ from -0.46 to -5.77 kcal/mol. This range of strength of the water–substrate interaction approximately corresponds to a variation of the substrate from hydrocarbonlike to metallic. The LJ (9-3) potential with $\sigma=2.5$ Å results from the integration over a substrate with flat, nonspherical surface and uniformly distributed LJ (12-6) centers with $\sigma=3.5$ Å. In order to estimate the effect of curvature on the water–substrate interaction, numerical integrations over LJ (12-6) centers surrounding spherical cavities of different radii were done with the same fixed density of the substrate. The value of σ remains practically the same as for the flat substrate ($\sigma=2.5$ Å), whereas the well-depth increases approximately by a factor of 2.5 ($R_c=6$ Å), 1.80 ($R_c=9$ Å), 1.54 ($R_c=12$ Å), and 1.41 ($R_c=15$ Å). Initial configurations were produced by equilibration in the NPT ensemble for bulk water and in the NVT ensemble for water in cavities with various numbers of molecules.

The chemical equilibration of the water in the cavity with bulk water was provided by simulations in the Gibbs ensemble. In order to determine the density of the cavity water in equilibrium with the bulk, an essential number of transfers between the two simulated systems must be provided. The insertion of molecules was done as follows: (a) a position and orientation for insertion was chosen randomly; (b) the distances between the atoms of the inserted molecule and the atoms of its neighbors were calculated; (c) if at least one of these distances is shorter than some ''critical'' value, the new configuration is rejected immediately, otherwise energetical calculations follow. The choice of the ''critical'' interatomic distances was done on the basis of the different pair distribution functions, calculated for water both in the bulk and in the cavity. They correspond to the largest interatomic distances, which are never observed in long-term ca-

nonical MC simulations. These values are not very sensitive to the water density and were fixed at 2.35 Å for the O–O distance, 1.40 Å for the O–H distance, and 1.30 Å for the H–H distance. Similarly, in the case of insertions in the cavity, a ''critical'' value of 2.0 Å was chosen for the oxygen–wall distance. Another problem in the Gibbs ensemble simulation of two liquid dense phases is the deletion of molecules. The energetic distribution of water molecules in the dense phase typically posses a maximum at approximately -20 kcal/mol, whereas the lowest energies of randomly inserted molecules are usually higher than -12 to -13 kcal/mol. This means that it is most efficient to use for the deletion water molecules from the high-energy tail of the distribution. In this case the probability of acceptance of the new configuration must be corrected by multiplying it with some factor P_c, which is equal to the probability to find water molecules with energies, higher than some chosen ''cutoff'' value U_c. This value was chosen between -10 and -13 kcal/mol, depending on the system. The corresponding values of P_c are in the range of 0.005–0.1. P_c was calculated before each set of attempts to transfer molecules and running averages were used in order to improve the accuracy of P_c during the simulations, For a fixed value of U_c a single value of P_c had to be calculated for bulk water, whereas for the water in the cavity a set of $P_c(N)$ was used. With a decreasing fraction of water molecules, used for deletion, the efficiency of successful deletions improves, whereas the accuracy of the correction factor for the acceptance probability decreases. This effects the length of the equilibration, but there were no other noticeable changes. Another important factor is the choice of the appropriate ratio of moves within the simulation boxes and between them. The equilibration process becomes unstable, when the thermal equilibration of the two boxes between successful transfers is not sufficient.

One Gibbs ensemble simulation step consists of (1) thermal equilibration with 1000 MC moves (translational and rotational) in both systems and 2 attempts to vary the volume of the bulk phase in order to impose constant pressure; with acceptance probabilities between 40% and 50% in all cases; (2) chemical equilibration of the two systems by the transfers of randomly chosen molecules; a series of 0.5×10^5 to 1.5×10^6 attempts yields a probability of a few to 50% to get one successful transfer, depending on the state of the systems. If the transfer is accepted, the number of water molecules in the cavity changes accordingly. The transfer from and to the bulk actually is ignored, because it is simulated at fixed P and T. In order to be sure, that the system is not trapped in some metastable state, we always start from two different initial configurations of water in the cavity—with high and low density. For the cavity with a radius $R_c = 12$ Å this corresponds to $N>100$ and $N=20-25$ molecules, respectively. In any case the number of successful transfers was greater than $2\langle N\rangle$, where $\langle N\rangle$ is the final average number of water molecules in the cavity. This means a sharp increase of the simulation time with increasing pore size.

Increasing the temperature from 300 K to 350 K results in an essential speed up (a few times) of the equilibration process, whereas its decrease to 275 K results in a slowing down of the same order.

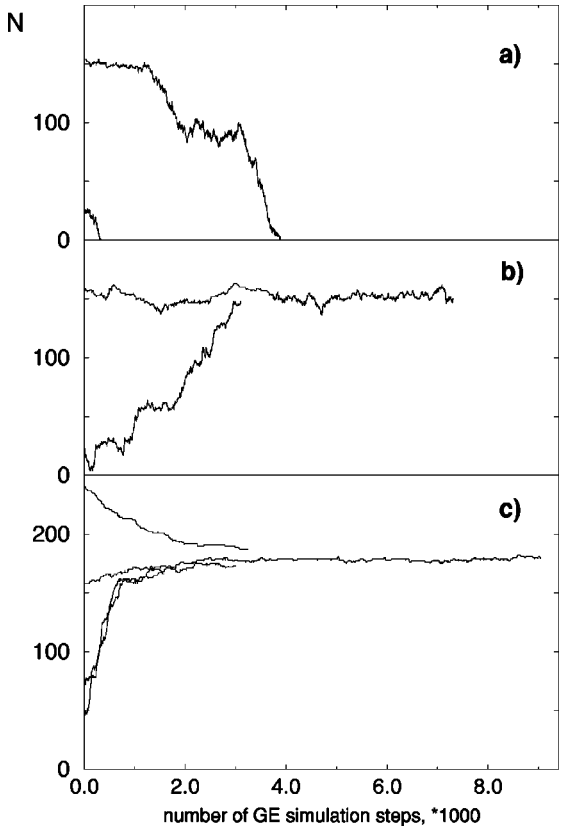

FIG. 1. Change of the number of water molecules in spherical cavities ($R_c=12$ Å, $T=300$ K) during the equilibration period of some Gibbs ensemble MC simulations. Water–substrate interaction (a) $U=-1.16$ kcal/mol; (b) $U=-1.93$ kcal/mol; (c) $U=-4.62$ kcal/mol.

III. RESULTS

A. Gibbs ensemble simulations

Equilibration processes are presented for some systems in Fig. 1. For weak water–substrate interactions [Fig. 1(a)] the cavity empties during the equilibration process, whereas for stronger water–substrate interaction [Figs. 1(b) and 1(c)] the cavity fills with water molecules. An equilibrium value of the number of water molecules in the cavity is obtained from long term runs. The dependence of this number on the well-depth U of the water–substrate interaction for different cavities is presented in Fig. 2. In this figure the data points with $N=0$, representing finally empty cavities, correspond to cavities with $R_c=12$ Å, $U=-0.46$; -0.77; -1.15, and -1.54 kcal/mol, and with $R_c=6$ Å, $U=-1.93$ kcal/mol. For most of the simulated systems the final number of water molecules in the cavity did not depend on its initial number. The only exception is the system with $R_c=12$ Å and $U=-1.54$ kcal/mol. It becomes empty when the simulation starts from a low-density initial configuration (as it is shown in Fig. 2). For a high-density initial configuration, the number of water molecules varies in the range from 80 to 150 molecules without a tendency to reach equilibrium even during long-term calculations (few times longer than typical calculation for such systems).

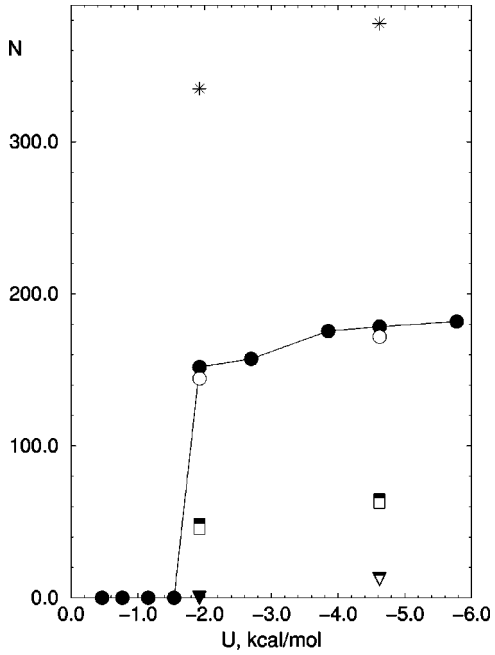

FIG. 2. Dependence of the equilibrium number of water molecules in spherical cavities on the water–substrate interaction well-depth U: stars, $R_c=15$ Å; circles, $R_c=12$ Å; squares, $R_c=9$ Å; triangles, $R_c=6$ Å (closed symbols, $T=300$ K; open symbols, $T=350$ K).

The data presented in Fig. 2 evidence the existence of some critical value of the water–substrate interaction parameter U. Liquid water exists in spherical cavities with $R_c=12$ Å only if $U<-1.5$ kcal/mol and this critical value becomes more negative for smaller cavities (see the results for cavities with $R_c=6$ Å, Fig. 2). The above mentioned instability in the equilibration process for the system with $R_c=12$ Å and $U=-1.54$ kcal/mol may be attributed to its proximity to the boundary value.

When discussing the influence of the cavity size on the water density in identical substrate materials, the effect of curvature on the water–substrate potentials (as discussed in Sec. II) must be taken into account. This results in a scaling of the parameter U of Fig. 2 by a factor of 1.62 for a cavity with $R_c=6$ Å, by a factor of 1.17 for a cavity with $R_c=9$ Å and by a factor of 0.92 for a cavity with $R_c=15$ Å (using the cavity with $R_c=12$ Å as the reference system).

The average density of the water in the cavities depends essentially on the parameter U. It increases by 12%, 18%, and 34% for cavities with $R_c=15$ Å, $R_c=12$ Å, and $R_c=9$ Å, respectively, when U changes from -1.93 to -4.62 kcal/mol. A temperature increase from 300 K to 350 K causes a slight decrease of the number of water molecules in the cavity by a few %. Estimates of the average water density in small cavities are subject to a certain arbitrariness in the determination of the volume which is accessible to the water. In Table I values of the water density ρ are presented which were obtained by assuming that the water occupies a sphere with radius $R=R_C-\sigma/2$, where $\sigma=2.5$ A corresponds to the water–substrate interaction potential.

TABLE I. Parameters of the simulated systems: R_c, cavity radius; U, well-depth of the water–substrate potential; T, temperature; $\langle N\rangle$, equilibrated average number of water molecules in the cavity; ρ, average water density in the cavity.

System	R_c(Å)	$-U$ (kcal/mol)	T (K)	$\langle N\rangle$	ρ (g/cm^3)
1	15	4.62	300	375.6	1.03
2	15	1.93	300	338.4	0.93
3	12	4.62	300	178.3	1.02
4	12	4.62	350	171.1	0.98
5	12	5.77	300	181.6	1.04
6	12	3.85	300	175.5	1.01
7	12	2.69	300	157.2	0.90
8	12	1.93	300	151.8	0.87
9	12	1.93	350	144.2	0.83
10	9	4.62	300	64.9	0.99
11	9	4.62	350	62.5	0.96
12	9	1.93	300	48.4	0.74
13	9	1.93	350	45.2	0.69
14	6	4.62	300	12.1	0.81
15	6	4.62	350	11.7	0.78

B. Structural properties of water in spherical cavities

The integer values closest to the average numbers $\langle N\rangle$ of water molecules given in Table I were used for the simulation and analysis of the structural and dynamical properties of water. MC simulations were done in the canonical NVT ensemble, structural analysis was performed every 1000 MC steps during runs of 2×10^5 configurations. In Fig. 3 water density profiles along the cavity radius are presented. The water density was calculated based on the positions of the centers of the O and H atoms. Strong layering of water exists in all systems and a temperature increase to 350 K has no essential effect on it. Even for the weakest water–substrate interaction for which water still exists in the cavity ($U=-1.93$/kcal/mol), the water density profile exceeds 2.5 g/cm^3 in the first outer layer [Fig. 3(f)]. This means that water can exists in cavities (in equilibrium with the bulk water at the given P and T) only, when prominent layers are formed. For small cavities ($R_c=6$ Å) only one water layer remains [Fig. 3(a)]. The analysis of the structural properties of the cavity water was done separately for the different water layers. The layer thiknesses were determined by the distances between the minima in the water density profile (Fig. 3). The properties of the water layers are described in Table II.

When calculating the pair correlation functions of a liquid in a confined geometry, the excluded volume effect must be taken into account.[82] In our case, the spherical shells, constructed around given sites to determine radial distribution functions are overlapping only partly the spherical volume of radius R_S occupied by the molecules in the cavities. Uncertainties in the determination of R_S enter into the computation of this reduced volume. We choose this parameter as the largest distance from the center of cavity, where the considered sites were observed during the simulation. The same values R_S were used for the determination of the average density of the sites to normalize the pair correlation functions. The values of R_S for O and H atoms were calculated in advance. These values of R_S are lower than the cavity radius

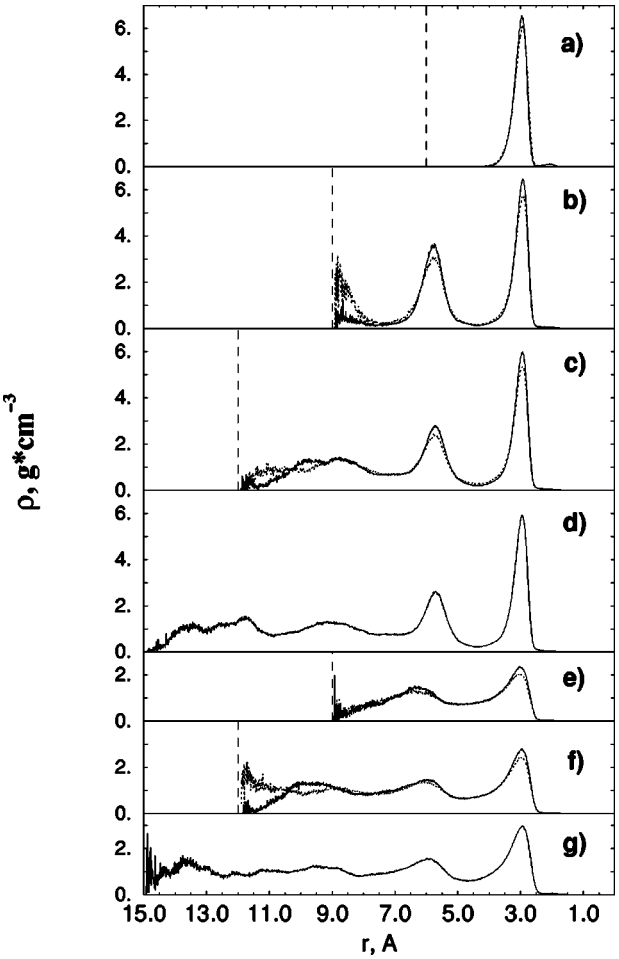

FIG. 3. Water density along the cavity radius: (a) $R_c=6$ Å; $U=-4.62$ kcal/mol (system Nos. 14 and 15, Table I); (b) $R_c=9$ Å; $U=-4.62$ kcal/mol (Nos. 10 and 11); (c) $R_c=12$ Å; $U=-4.62$ kcal/mol (Nos. 3 and 4); (d) $R_c=15$ Å; $U=-4.62$ kcal/mol (No. 1); (e) $R_c=9$ Å; $U=-1.93$ kcal/mol (Nos. 12 and 13); (f) $R_c=12$ Å; $U=-1.93$ kcal/mol (Nos. 8 and 9); (g) $R_c=15$ Å, $U=-1.93$ kcal/mol (No. 2). Solid lines, $T=300$ K; dotted lines, $T=350$ K. Vertical dashed lines indicate the center of cavities.

R_c by 2.2–2.4 Å for O atoms and by 1.4–1.5 Å for H atoms in all cases. Two different approaches were used to calculate the pair correlation functions in the water layers: (a) at least one of the sites is in the analyzed layer; (b) both sites are in the analyzed layer. In the latter case also the volume of the other layers was excluded in the calculations.

Radial distribution functions $g_{O-O}(r)$ in the cavities and in bulk water are presented in Fig. 4. The changes which appear in the cavities at large r [Figs. 4(a) and 4(b)] reflect directly the strong layering of water near the cavity wall. In general, $g_{O-O}(r)$ approaches the bulk function with decreasing water–substrate interaction. However, some peculiarities are observed for all systems: the appearance of additional intensity on the higher r side of the first maximum; a decrease of the second (at 4.4 Å) and third (at 6.7 Å) maximum; the appearance of an additional maximum around 5.45 Å. An analysis of the radial distribution functions in different water layers shows that these new features correspond mainly to correlations within the first water layer. In Fig. 5 radial distribution functions $g_{O-O}(r)$ are presented for the first, outer layers of water in different cavities. The differences of the $g_{O-O}(r)$ to bulk water [Fig. 5(e)] increase with strengthening of the water–substrate interaction [Figs. 5(d) and 5(c)] and decreasing cavity size [Figs. 5(c) and 5(b)]. They are most pronounced when only atoms inside the first layer are considered [Fig. 5(a)]. The tetrahedral structure of water is distorted in the cavities: the shift of the second maximum of $g_{O-O}(r)$ by 0.15 Å corresponds to a change of the OOO-angle from 107° to 102°. The shift of the third maximum by 0.4 Å reflects still stronger distortions of the long-range tetrahedral structure of water in the cavities. The position of the new maximum of $g_{O-O}(r)$, appearing at 5.45 Å, corresponds to a doubling of the first maximum distance of 2.75 Å. All above mentioned features of the $g_{O-O}(r)$ show that the tetrahedral structure of water diminishes in cavities and some features of a square lattice structure in the outermost water layer appear.

For the analysis of the orientational ordering of water molecules in cavities $\cos\alpha$-distributions were calculated for the angles α between the intramolecular OH-vectors and the radius vector (Fig. 6) as well as between the dipole moment and the radius (Fig. 7). In the small cavity ($R=6$ Å) with a single water layer all water molecules have an orientation of the OH-vector along the radius away from the cavity center with $\alpha=0°$ or with $\alpha=114°$, close to the tetrahedral value [Fig. 6(a)]. This is confirmed by an analysis of the density profile of H atoms along the cavity radius [Fig. 8(a)]: the additional maximum at 2 Å from the surface corresponds to an orientation of the OH bonds away from the cavity center along the radius (its distance to the maximum in the oxygen density profile is equal to 1 Å). This structure results in two preferential orientations of the dipole moment with respect to the cavity radius: with $\alpha=66°$ and $\alpha=125°$ [Fig. 7(a)]. The appearance of the second water layer with increasing cavity radius leads to essential changes of the orientational ordering of the water molecules. Now a large number of OH-vectors is directed towards the center of the cavity and normal to the radius vector [Figs. 6(b)–6(f)]. This results in the appearance of a broad distribution around orientations of the dipole moment normal to the cavity radius [Figs. 7(b)–7(f)].

An analysis of the orientational ordering in different water layers (Figs. 9 and 10) shows that the discussed orientational ordering is caused mainly by the first outer water layer which contains most of the water molecules (Table II). The orientational ordering in the second layer [Fig. 9(b), Fig. 10(b)] is similar to the ordering in the single layer of the small cavity. Some preferential orientation of the OH bonds remains even for the inner water [Fig. 9(a)]. The degree of orientational ordering increases with the strengthening of the water–substrate interaction (Fig. 6, Fig. 7). For stronger interactions the preferential orientations of the OH bonds are reflected even in the H atom density distribution (Fig. 8). The two maxima around 4 Å and 5 Å from the cavity surface correspond to the OH bond orientation in the first and second water layer, respectively. They reflect a preferential orientation of the OH bonds of these layers towards each other. In the angular distributions this corresponds to configurations with $\cos\alpha=-1$ [Fig. 9(c)] and $\cos\alpha=+1$ [Fig. 9(b)].

An analysis of the energetic distributions (Table II) in

TABLE II. Some properties of the water layers in the spherical cavities. I, number of the system from Table I; II, numbers of the water layer, 4 corresponds to the complete cavity; III, location of the water layer from the cavity surface, in Å (compare Fig. 3); IV, fraction of water in the layer, in %; V, molecules with less than 3 H-bonds, %; VI, molecules with 3 H-bonds, % VII, molecules with 4 H-bonds, %; VIII, molecules with more than 4 H-bonds, %; IX, averaged water–water interaction per molecule, kcal/mol; X, averaged water–substrate interaction per molecule, kcal/mol; XI, averaged total energy of interaction per molecule, kcal/mol.

I	II	III	IV	V	VI	VII	VIII	IX	X	XI
System (Table I)	Layer	Layer position	% of water in layer	% of molecules with less than 3H-bonds	% of molecules with 3H-bonds	% of molecules with 4H-bonds	% of molecules with more than 4H-bonds	Water–water inter-action	Water–substrate inter-action	Total inter-action
1	1	2.43–4.36	53.4	18.5	43.3	32.9	5.3	−8.49	−2.13	−10.62
	2	4.36–7.11	28.7	8.5	29.7	45.6	16.1	−9.93	−0.51	−10.44
	3	7.11–15.00	17.9	10.5	33.0	44.5	11.9	−9.85	−0.14	−9.99
	4	···	···	14.2	37.3	38.6	9.6	−9.14	−1.31	−10.45
2	1	2.27–4.59	52.2	22.6	45.7	28.0	3.6	−8.24	−0.80	−9.04
	2	4.59–8.03	33.6	9.6	31.5	44.8	14.1	−9.79	−0.19	−9.98
	3	8.03–15.00	14.3	11.4	34.1	43.9	10.8	−9.74	−0.05	−9.79
	4	···	···	16.7	39.3	35.9	8.2	−8.99	−0.48	−9.47
3	1	2.42–4.37	63.3	19.3	45.1	31.0	4.7	−8.31	−2.13	−10.44
	2	4.37–7.20	28.2	8.4	29.2	44.9	17.5	−9.91	−0.51	−10.42
	3	7.20–12.00	8.5	10.0	33.4	44.5	12.0	−9.84	−0.16	−10.00
	4	···	···	14.4	39.6	36.1	8.9	−8.86	−1.53	−10.39
4	1	2.38–4.36	63.5	27.6	44.6	24.4	3.3	−7.80	−2.11	−9.91
	2	4.36–7.06	27.2	13.8	33.4	38.8	14.0	−9.32	−0.52	−9.84
	3	7.06–12.00	9.3	16.5	36.5	36.9	10.1	−9.22	−0.17	−9.39
	4	···	···	22.8	40.8	29.5	6.9	−8.34	−1.50	−9.84
8	1	2.29–4.29	64.4	25.1	46.1	25.7	3.1	−8.13	−0.78	−8.91
	2	4.29–7.99	29.5	9.7	31.8	45.2	13.2	−9.82	−0.18	−10.00
	3	7.99–12.00	6.1	9.8	31.9	45.9	12.4	−9.89	−0.05	−9.94
	4	···	···	19.6	40.1	32.7	6.7	−8.71	−0.57	−9.28
9	1	2.24–4.80	63.7	34.4	43.5	19.6	2.4	−7.47	−0.77	−8.24
	2	4.80–7.57	28.2	15.3	35.7	38.4	10.6	−9.15	−0.19	−9.34
	3	7.57–12.00	8.1	16.4	37.5	37.1	9.0	−9.18	−0.06	−9.24
	4	···	···	27.4	40.8	26.4	5.2	−8.08	−0.55	−8.63
10	1	2.41–4.38	78.5	23.6	48.0	25.6	2.9	−7.97	−2.14	−10.11
	2	4.38–7.56	21.4	7.9	28.7	46.2	17.4	−10.02	−0.52	−10.54
	3	7.56–9.00	0.1	18.7	40.0	35.2	6.1	−8.33	−0.18	−8.51
	4	···	···	20.2	43.9	30.0	5.9	−8.38	−1.82	−10.20
11	1	2.34–4.39	78.3	29.0	46.7	21.8	2.6	−7.51	−2.12	−9.63
	2	4.39–7.40	21.3	12.0	31.9	40.4	15.8	−9.39	−0.52	−9.91
	3	7.40–9.00	0.4	15.1	36.2	36.3	12.3	−8.60	−0.18	−8.78
	4	···	···	25.7	44.0	26.1	5.4	−7.94	−1.75	−9.69
12	1	2.26–4.88	79.5	31.0	48.1	19.0	1.9	−7.64	−0.78	−8.42
	2	4.88–7.56	19.9	9.0	31.0	46.7	13.2	−9.67	−0.20	−9.87
	3	7.56–12.00	0.6	7.7	30.2	48.6	13.5	−9.97	−0.08	−10.05
	4	···	···	26.5	44.5	24.7	4.2	−8.06	−0.66	−8.72
13	1	2.29–5.02	80.7	42.4	42.2	14.0	1.5	−7.01	−0.76	−7.77
	2	5.02–7.56	18.7	16.5	36.8	37.3	9.5	−8.94	−0.19	−9.13
	3	7.56–9.00	0.6	14.5	34.4	40.2	10.9	−9.12	−0.08	−9.20
	4	···	···	37.3	41.1	28.7	3.1	−7.48	−0.62	−8.10
14	1	2.41–4.75	100	25.6	69.5	4.9	0.1	−7.36	−2.18	−9.54
15	1	2.41–5.20	100	35.5	58.7	5.7	0.1	−6.84	−2.16	−9.00
		bulk (300 K)	100	12.0	35.3	43.9	8.7	−9.95	0.00	−9.95
		bulk (350 K)	100	19.9	38.6	34.6	7.0	−9.23	0.00	−9.23

different water layers shows weakening of the water–water interaction in the first, outer layer in all systems, whereas for the inner water it is closer to the bulk value. In general, the total energy of interaction (water–water plus water–substrate interaction) becomes more negative along the cavity radius towards the surface for strong water–substrate interaction, and it becomes less negative for weak water–substrate interaction (Table II).

For the analysis of the number of H-bonds per molecule an energetic criterion is used; a pair of water molecules is considered to be bonded when their pair interaction is stronger than −2.25 kcal/mol (see Fig. 10). The number of H-bonds decreases sharply in the first layer and this trend becomes more pronounced for smaller cavities and weaker water–substrate interactions (Table II). Hydrogen bonding of inner water is close to the bulk behavior. In the second water layer, which ''connects'' outer and inner water, an increase of configurations with more than 4 H-bonds may be noted.

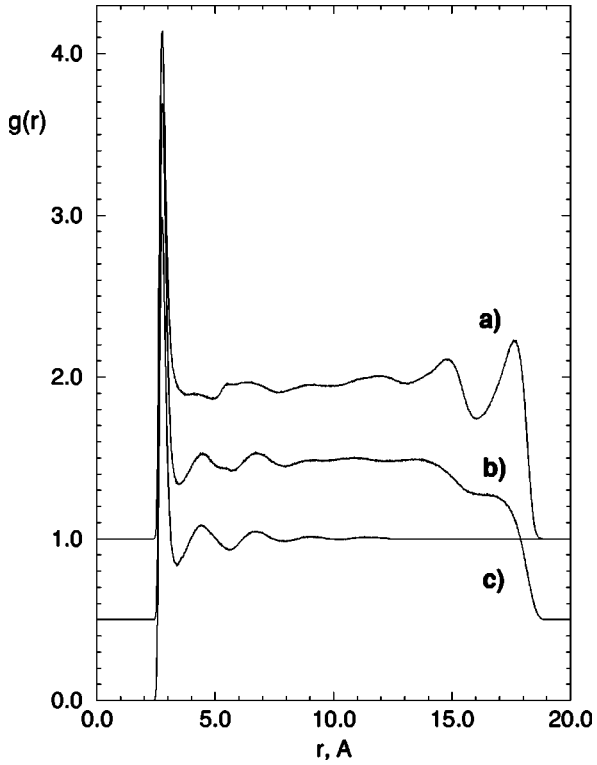

FIG. 4. Radial distribution functions $g_{O-O}(r)$ ($T=300$ K); (a) water in a spherical cavity [$R_c=12$ Å, $U=-4.62$ kcal/mol (No. 5), shifted up by 1.0]; (b) water in a spherical cavity [$R_c=12$ Å, $U=-1.93$ kcal/mol (No. 8), shifted up by 0.5]; (c) bulk water.

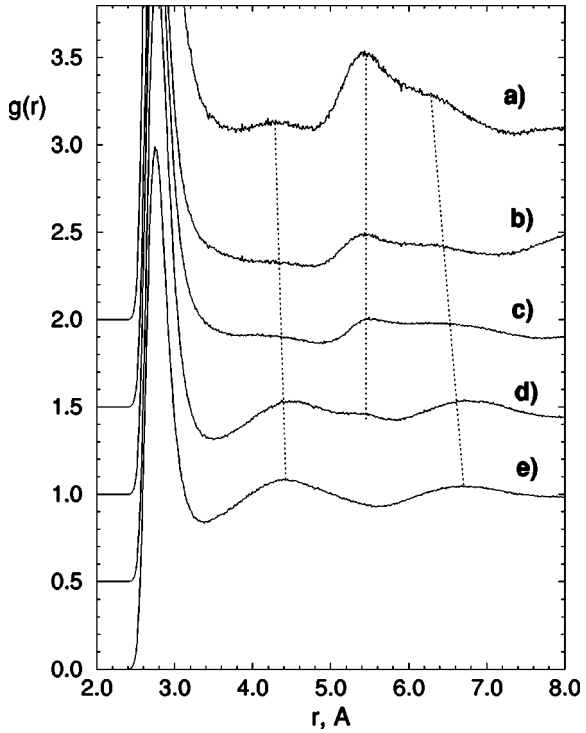

FIG. 5. Radial distribution functions $g_{O-O}(r)$ ($T=300$ K): (a)–(d) water in spherical cavities, (e) bulk water; the curves are shifted by 0.5 successively: (a) $R_c=9$ Å, $U=-4.62$ kcal/mol (No. 10), both oxygen atoms are in the first layer; (b) $R_c=9$ Å, $U=-4.62$ kcal/mol (No. 10); (c) $R_c=12$ Å, $U=-4.62$ kcal/mol (No. 3); (d) $R_c=12$ Å, $U=-1.93$ kcal/mol (No. 8); (b)–(d) at least one of the oxygens is in the first layer. Dotted lines show the shifts of the main maxima of $g_{O-O}(r)$.

C. Diffusivity of water in spherical cavities

MD simulations of water in spherical cavities with $R_c=12$ Å, $U=-4.62$ kcal/mol, and $R_c=12$ Å, $U=-1.93$ kcal/mol were done (for systems No. 3 and 8 with the appropriate numbers of water molecules from the Gibbs ensemble simulations at 300 K) in order to analyze the diffusivity of water. Mean-square displacements of oxygen atoms as a function of time for these systems are presented in Fig. 11. For long times, $\langle \Delta r^2(t) \rangle$ reaches a plateau, which indicates the confinement in the cavity. The isotropic short-time self-diffusion coefficients D were determined from the intermediate linear parts of the presented dependencies. The obtained average values are $D=1.85\times10^{-3}$ m^2/s ($R_c=12$ Å, $U=-4.62$ kcal/mol) and $D=2.93\times10^{-3}$ m^2/s ($R_c=12$ Å, $U=-1.93$ kcal/mol). In both cases the self-diffusion coefficient is lower than the bulk value $D=3.61\times10^{-3}$ m^2/s, obtained at 300 K with the same parameters of interaction and at bulk density. The general decrease of water diffusivity may be noted.

In Fig. 12 profiles of the self-diffusion coefficient along the cavity radius are shown. The diffusivity roughly shows an anticorrelation to the density profile: low diffusion coefficients in the region of the density profile maxima. This indicates some kind of trapping in the two outer adsorption layers. This effect is less clear in the less structured system No. 8. Nevertheless, self-diffusion coefficient never achieved bulk value even for the weakest water–substrate interaction ($U=-1.93$ kcal/mol), for which liquid water still exists in the cavity. The details of the observed dependencies may be rather involved and due to competing influences: besides the influence of the layering, which leads to a decrease of diffusivity, an increase is produced by a strong decrease of the H-bonding in the outer layer as well as an increased number of molecules with five neighbors in the intermediate water shell (Table II). This would be in accord with observations in bulk water.[83] In summary, a strong influence of the water–substrate interaction and the resulting structural changes on the water diffusivity is observed. This underlines the necessity for Gibbs ensemble simulations to determine the correct water density in the cavities.

IV. DISCUSSION

Equilibration with a bulk reservoir is the crucial problem in the simulation of water in confined geometries, since the structural and dynamical properties of water are highly sensitive to its density. In this paper we discuss the application of GE simulations for the equilibration of water in spherical cavities with bulk water. The main problem in GE simulations is connected with the necessity to provide the deletion of a molecule in one box and its insertion in another box in one move. For dense and highly associated systems like liquid water, efficiencies of both insertion and deletion are very low. In order to improve the efficiency of the insertions we used an analysis of the interatomic distances in the new configurations. This analysis includes not only O···O distances (like in other simulations of such kind),[45,79] but also O···H distances. It allows to exclude new configuration at an early

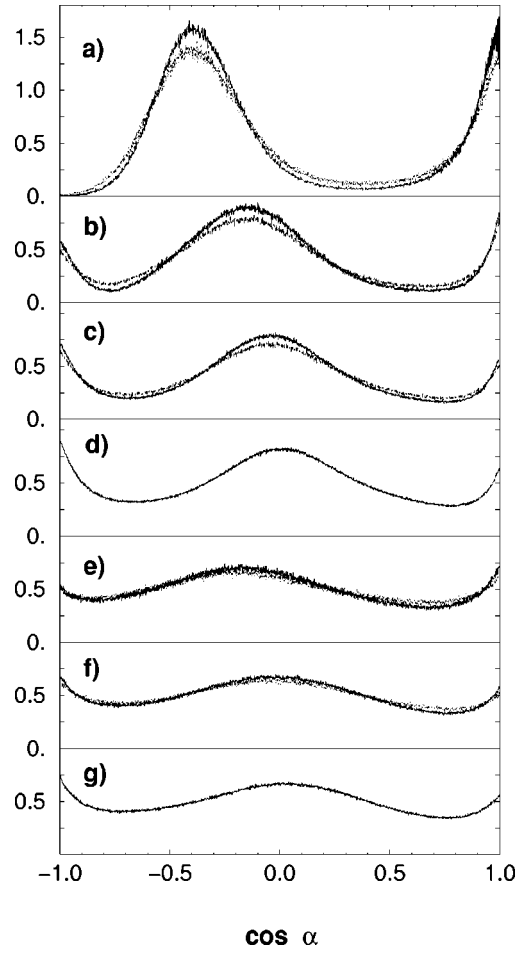

FIG. 6. Angular distributions: α is the angle between the OH vector and the cavity radius vector. (a) $R_c=6$ Å; $U=-4.62$ kcal/mol (Nos. 14 and 15); (b) $R_c=9$ Å; $U=-4.62$ kcal/mol (Nos. 10 and 11); (c) $R_c=12$ Å; $U=-4.62$ kcal/mol (Nos. 3 and 4); (d) $R_c=15$ Å; $U=-4.62$ kcal/mol (No. 1); (e) $R_c=9$ Å; $U=-1.93$ kcal/mol (Nos. 12 and 13); (f) $R_c=12$ Å, $U=-1.93$ kcal/mol (Nos. 8 and 9); (g) $R_c=15$ Å, $U=-1.93$ kcal/mol (No. 2). Solid lines, $T=300$ K; dotted lines, $T=350$ K.

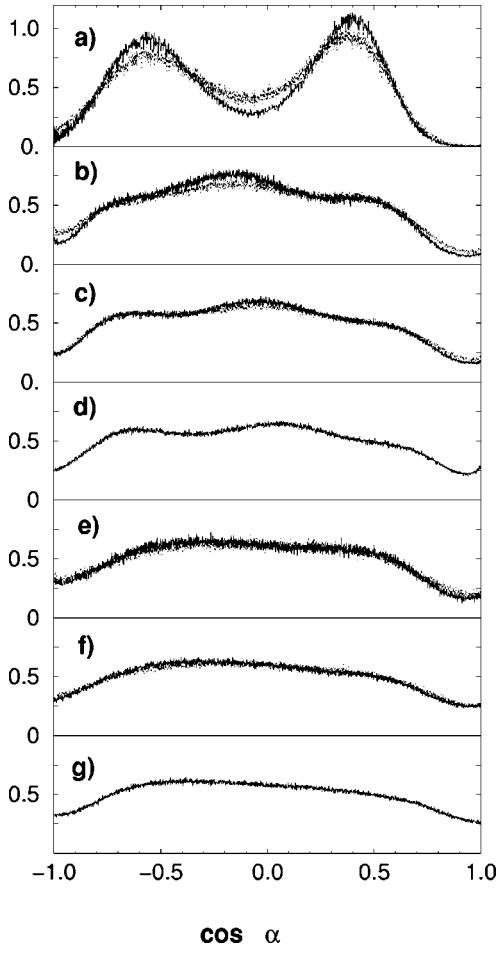

FIG. 7. Angular distributions: α is the angle between the dipole moment vector and the cavity radius vector. (a)–(g) correspond to the same systems as in Fig. 6.

stage of analysis. In order to improve the efficiency of water molecule deletions we used a bias method, which is based on the choice of the water molecules from the high-energy tail of the energetic distribution. Use of these two techniques allowed to improve the efficiency of the simulations and to achieve equilibration of the number of water molecules in pores (Fig. 1).

This successful application of GE for the equilibration of two dense water systems shows perspectives for its use in simulations of complex aqueous systems. But even for simple aqueous solutions simulations in the usual canonical ensemble or MD simulations may not provide accurate equilibration. The system may be easily trapped in some metastable state and, for example, a possible aggregation of the solute molecules will never be observed due to the finite time of calculations. It may also be important in simulations of water in biological membranes, since many possible water distributions are unachievable in the course of usual MC or MD simulations. Water molecule transfers between different parts of the simulated system will provide the necessary chemical equilibration. The Gibbs ensemble may also be extended to simulations of liquid–liquid equilibria of aqueous solutions and, eventually, even of pure water at low temperatures (near the conjectured second critical point in supercooled water).[84]

The observed emptying of the pores at weak water–substrate interactions (Fig. 2) shows, that liquid water can not exist in small hydrophobic pores and that water sharply starts penetrating the pores at some critical level of water–substrate interaction. This agrees well with the experimental observations of water penetration into pores with different ratios of hydrophobic and hydrophilic groups.[5]

Based on the GE simulations we were able to obtain reliable data for different structural and dynamical properties of water in spherical pores. Contrary to previous simulations of water in spherical pores,[61–66] a strong layering of water near the pore wall is always observed. Even for the weakest water–substrate interaction the local water density develops a pronounced first maximum. This means, that liquid water can exist in spherical cavities only when forming prominent layers.

The analysis of the obtained density distributions (Fig. 3, Fig. 8), orientational distributions (Fig. 9, Fig. 10), and energetic calculations (Table II) allows us to divide up the pore water into three distinct parts: water near the pore wall (first outer layer, 0–4.5 Å from the surface, ''bound'' water), wa-

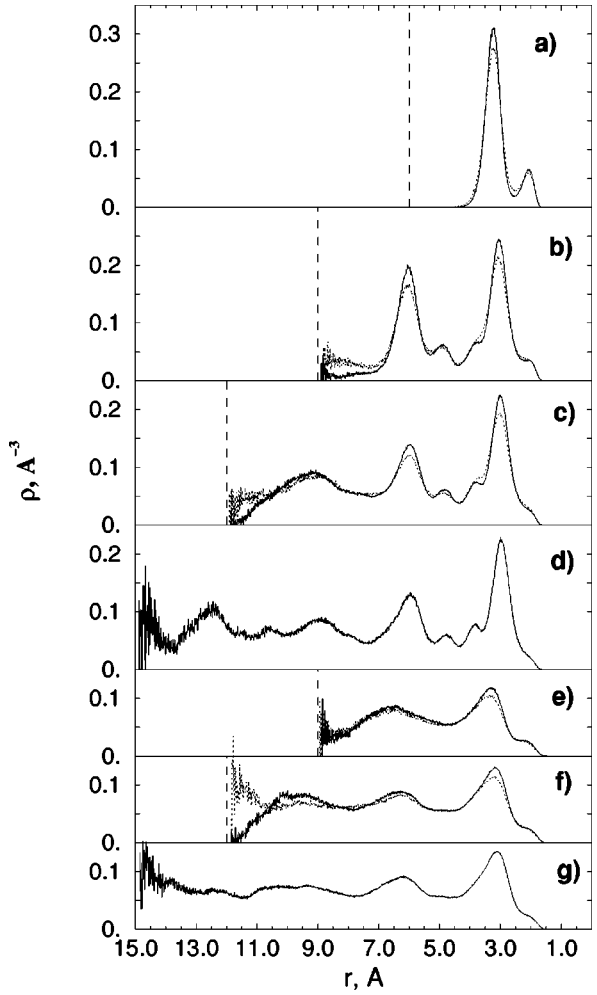

FIG. 8. Hydrogen atom density profiles along the radius of the spherical cavities. (a)–(g) correspond to the same systems as in Fig. 6.

ter in the center of the pore (''inner'' water), and ''connecting'' water between them (second water layer, 4.5–7 Å from the surface).

The main properties of the ''inner'' water are close to the bulk. The ''connecting'' water shows specific orientational ordering with a preference for orientations of OH bonds towards ''bound'' water along the cavity radius and towards the ''inner'' water with an angle, which is close to the tetrahedral value. Another peculiarity of the ''connecting'' water is its increased number of configurations with more than 4 H-bonds per molecule.

The ''bound'' water is strongly distorted with respect to the bulk water. The average water–water interaction is weaker and the number of H-bonds decreases appreciably (Table II). The orientational ordering reflects preferential orientations of the OH bonds normal to the cavity radius or along it. The radial distribution function $g_{O-O}(r)$ of ''bound'' water differs strongly from both the bulk water and the other water layers in the cavity. The additional intensity at the high r side of the first peak of $g_{O-O}(r)$ is similar to the observed changes in bulk water at high pressures.[85] The appearance of an additional maximum in $g_{O-O}(r)$ around 5.45 Å, which corresponds to the doubling of the position of the first maximum, reflects distortion of the tetrahedral water

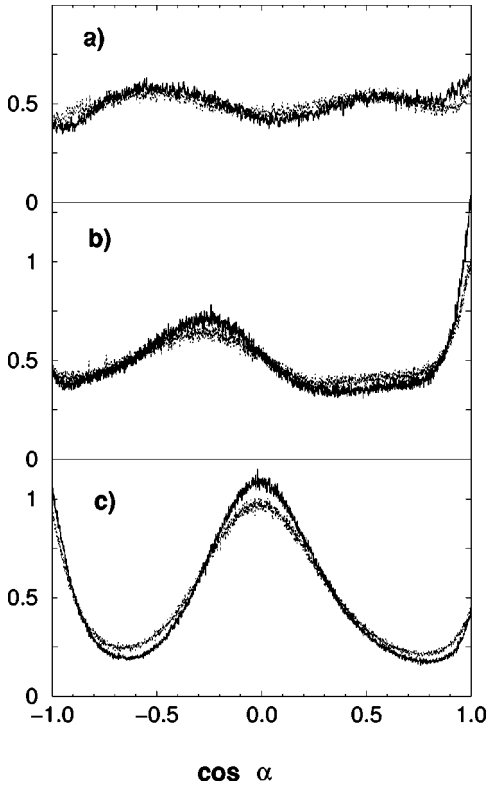

FIG. 9. Angular distributions: α is the angle between the OH vectors and the cavity radius. $R_c = 12$ Å; $U = -4.62$ kcal/mol; $T = 300$ K (No. 3). (a) Inner layer; (b) intermediate layer; (c) outer layer.

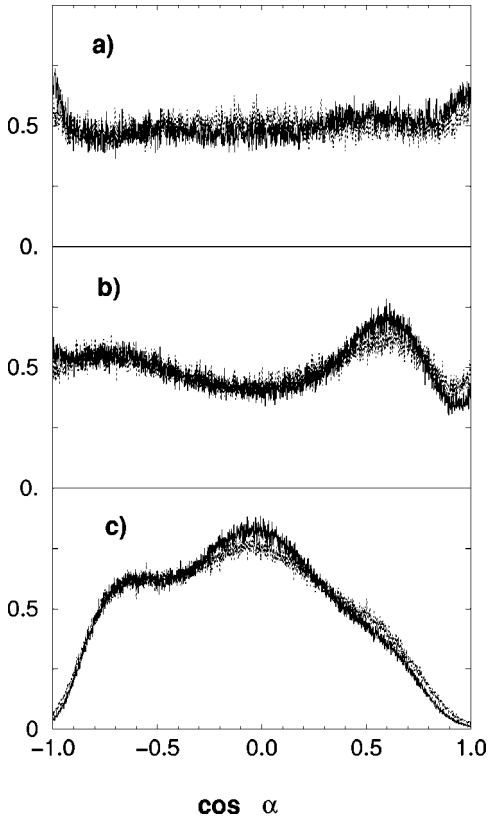

FIG. 10. Angular distributions: α is the angle between the dipole moment and the cavity radius. Same presentation as in Fig. 9.

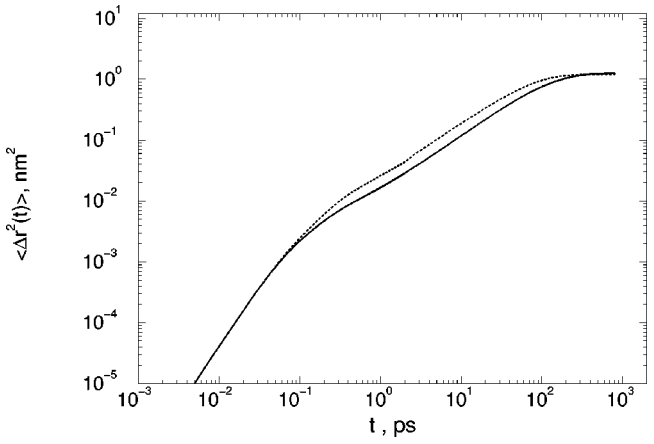

FIG. 11. Mean-square displacements of oxygen atoms as a function of time in spherical cavities with $R_c = 12$ Å, $U = -4.62$ kcal/mol (solid line), $U = -1.93$ kcal/mol (dotted line). Note the logarithmic scales.

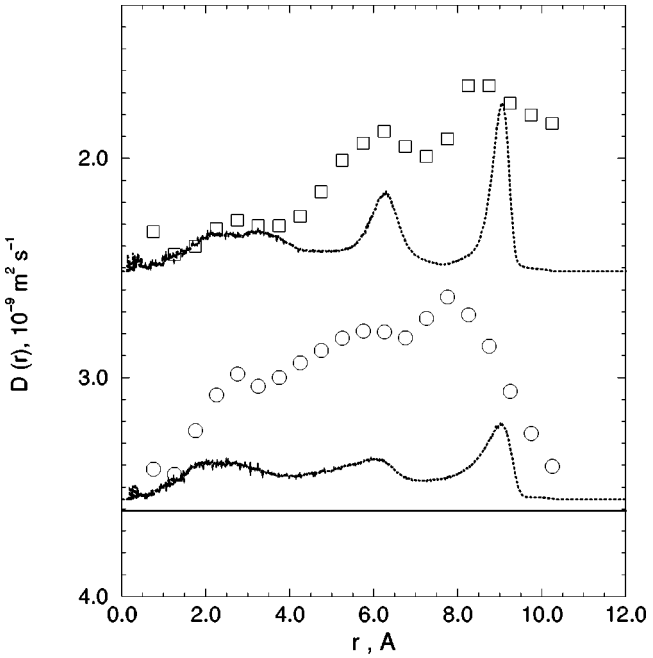

FIG. 12. Dependence of the self-diffusion coefficient of water molecule on its distance from the center of the spherical cavity: $R_c = 12$ Å; $T = 300$ K; circles, $U = -4.62$ kcal/mol (No. 3), squares, $U = -1.93$ kcal/mol (No. 8). Solid line corresponds to the bulk water. Water density profiles of the corresponding systems are shown by dotted lines in arbitrary scales. Note the inverted scale for the diffusion coefficients.

structure towards a square lattice or towards the structure of high density ice with interpenetrating hydrogen bond network.[86] A similar maximum was observed in the radial distribution function of bulk water at high pressure[85] and in some simulations of water on a structured surface.[29,48] But in the latter case it reflected the definite structure of the surface, whereas here we used a smooth surface. The changes of $g_{O-O}(r)$ in the first outer layer with respect to the bulk reflect a decrease of the short-range order of ''bound'' water. This agrees well with experimental x-ray diffraction studies of water in pores.[3]

The single remaining water layer in the cavity with $R = 6$ Å, shows essentially the properties of ''bound'' water, but its orientational ordering is similar to the ordering of ''connecting'' water in larger cavities. For all simulated systems the structural properties of water in cavities are not very sensitive to a temperature increase from 300 K to 350 K.

In general, we observe two prominent water layers near the surface. The structural properties of the first layer differ strongly from the bulk, whereas ''inner'' water is close to the bulk. Changing the cavity size from 9 Å to 15 Å results in increase of the percentage of ''inner'' water, but the main properties of the different species of water remain unchanged. The obtained layering suggests to expect specific thermodynamical properties of the water within 7 Å from cavity surface. This agrees well with the experimentally obtained thickness of nonfreezable water in pores.[3,4,6,8,11,12,14]

The slowing-down of water diffusivity, obtained in our simulations, is in good agreement with experimental observations.[18–23] We obtained a decrease of the self-diffusion coefficient even for the lowest possible density of liquid water in the cavity. In view of the fact that the mobility of water molecules in the bulk liquid is strongly affected by the local density,[83] we suspect that the increased water diffusivity, obtained in some simulations[25–27,31,42,58,64] is not only connected to an inappropriate water–substrate interaction strength, but also to an inappropriate choice of the water density.

V. CONCLUSIONS

Simulations of water in spherical cavities in equilibrium with bulk water were done in the GE. The successful use of GE simulation method for this particular case shows that it may be used for simulations of water in various confined environments in equilibrium with bulk water and also for other kinds of coexisting dense water phases.

Liquid water exists in a spherical cavity only if its interaction with the surface exceeds some critical value. Strengthening of the water–surface interaction causes an increase of the average water density by more than 20%. The first two outer water layers (up to 7 Å from the surface) show specific structural properties, whereas the properties of inner water are close to the bulk. The diffusivity of water always decreases in spherical cavities with respect to the bulk.

ACKNOWLEDGMENTS

Support from the Graduiertenkolleg Struktur-Dynamik Beziehungen in mikrostrukturierten Systemen and from Fonds der Chemischen Industrie is gratefully acknowledged.

[1] D. C. Steytler, J. C. Dore, and C. J. Wright, J. Phys. Chem. **87**, 2458 (1983).
[2] D. C. Steytler and J. C. Dore, Mol. Phys. **56**, 1001 (1985).
[3] Y. P. Handa, M. Zakrewski, and C. Fairbridge, J. Phys. Chem. **96**, 8594 (1992).
[4] K. Overloop and L. Van Gerven, J. Magn. Reson., Ser. A **101**, 179 (1993).
[5] Y. Hirama, T. Takahashi, M. Nino, and T. Sato, J. Colloid Interface Sci. **184**, 349 (1996).
[6] E. W. Hansen, M. Stokler, and R. Schmidt, J. Phys. Chem. **100**, 2195 (1996).
[7] E. W. Hansen, E. Tangstad, E. Myrvold, and T. Myrstad, J. Phys. Chem. B **101**, 10709 (1997).

[8] K. Morishige and K. Nobuoka, J. Chem. Phys. **107**, 6965 (1997).
[9] J. M. Baker, J. C. Dore, and P. Behrens, J. Phys. Chem. B **101**, 6226 (1997).
[10] T. Takamuku, M. Yamagami, H. Wakita, Y. Masuda, and T. Yamaguchi, J. Phys. Chem. B **101**, 5730 (1997).
[11] K. Morishige and K. Kawano, J. Chem. Phys. **110**, 4867 (1999).
[12] C. Favire, D. Bellet, and G. Dolino, Eur. Phys. J. B **7**, 19 (1999).
[13] M.-C. Bellisent-Funel, J. Lal, and L. Bosio, J. Chem. Phys. **98**, 4246 (1993).
[14] K. Ishikiriyama and M. Todoki, Thermochim. Acta **256**, 213 (1995).
[15] T. Ishizaki, M. Maruyama, Y. Furukawa, and J. G. Dash, J. Cryst. Growth **163**, 455 (1996).
[16] T. Iiyama, K. Nishikawa, T. Suzuki, and K. Kaneko, Chem. Phys. Lett. **274**, 152 (1997).
[17] J. D. F. Ramsay, Adv. Colloid Interface Sci. **76–77**, 13 (1998).
[18] M.-C. Bellisent-Funel, S. H. Chen, and J.-M. Zanotti, Phys. Rev. E **51**, 4558 (1995).
[19] E. W. Hansen, R. Schmidt, M. Stockler, and D. Akporiae, Microporous Mater. **5**, 143 (1995).
[20] R. Kimmich, S. Stapf, and A. I. Maklakov, Magn. Reson. Imaging **14**, 793 (1996).
[21] J. Texeira, J.-M. Zanotti, M.-C. Bellisent-Funel, and S.-H. Chen, Physica B **234**, 370 (1997).
[22] S. Mitra, R. Mukhopadhyay, K. T. Pillai, and V. N. Vaidya, Solid State Commun. **105**, 719 (1998).
[23] M.-C. Bellisent-Funel, S. H. Chen, and J.-M. Zanotti, Phys. Rev. E **59**, 3084 (1999).
[24] B. Jonsson, Chem. Phys. Lett. **82**, 520 (1981).
[25] M. Marchesi, Chem. Phys. Lett. **97**, 224 (1983).
[26] R. Sonnenschein and K. Heinzinger, Chem. Phys. Lett. **102**, 550 (1983).
[27] G. Barabino, C. Gavotti, and M. Marchesi, Chem. Phys. Lett. **104**, 478 (1984).
[28] C. Y. Lee, J. A. McCammon, and P. J. Rossky, J. Chem. Phys. **80**, 4448 (1984).
[29] E. Spohr and K. Heinzinger, Chem. Phys. Lett. **123**, 218 (1986).
[30] J. P. Valleau and A. A. Gardner, J. Chem. Phys. **86**, 4162 (1987).
[31] E. Spohr and K. Heinzinger, J. Chem. Phys. **84**, 2304 (1986).
[32] O. A. Karim and A. D. J. Haymet, J. Chem. Phys. **89**, 6889 (1988).
[33] J. Hautman, J. W. Halley, and Y.-J. Rhee, J. Chem. Phys. **91**, 467 (1989).
[34] R. F. Cracknell, D. Nicholson, and N. G. Parsonage, Mol. Phys. **75**, 1023 (1992).
[35] A. Delville, J. Phys. Chem. **97**, 9703 (1993).
[36] D. E. Ulberg and K. E. Gubbins, Mol. Simul. **13**, 205 (1994).
[37] S. H. Lee and P. J. Rossky, J. Chem. Phys. **100**, 3334 (1994).
[38] D. E. Ulberg and K. E. Gubbins, Mol. Phys. **84**, 1139 (1995).
[39] X. Xia and M. L. Berkowitz, Phys. Rev. Lett. **74**, 3193 (1995).
[40] K. Heinzinger, Mol. Simul. **16**, 19 (1996).
[41] J. C. Shelley and G. N. Patey, Mol. Phys. **88**, 385 (1996).
[42] J. R. Grigera, S. G. Kalko, and J. Fischbarg, Langmuir **12**, 154 (1996).
[43] S. K. Das, M. M. Sharma, and R. S. Schechter, J. Phys. Chem. **100**, 7122 (1996).
[44] J. Forsman, B. Jonsson, and C. E. Woodward, J. Phys. Chem. **100**, 15005 (1996).
[45] Y. C. Kong, D. Nicholson, N. G. Parsonage, and L. Thomson, Mol. Phys. **89**, 835 (1996).
[46] E. Spohr, J. Chem. Phys. **106**, 388 (1997).
[47] J. C. Shelley, G. N. Patey, D. R. Berard, and G. M. Torrie, J. Chem. Phys. **107**, 2122 (1997).
[48] C. H. Bridgeman and N. T. Skipper, J. Phys.: Condens. Matter **9**, 4081 (1997).
[49] E. Spohr, J. Chem. Phys. **107**, 6342 (1997).
[50] M. Sakurai, H. Tamagawa, K. Ariga, T. Kunitake, and Y. Inoue, Chem. Phys. Lett. **289**, 567 (1998).
[51] E. Spohr, A. Trokhymchuk, and D. Henderson, J. Electroanal. Chem. **450**, 281 (1998).
[52] I.-C. Yeh and M. L. Berkowitz, J. Electroanal. Chem. **450**, 313 (1998).
[53] I.-C. Yeh and M. L. Berkowitz, Chem. Phys. Lett. **301**, 81 (1999).
[54] A. Ignaczak and J. A. N. F. Gomes, J. Mol. Struct.: THEOCHEM **464**, 227 (1999).
[55] M. Maddox, D. Ulberg, and K. E. Gubbins, Fluid Phase Equilibria **104**, 145 (1995).
[56] M. S. P. Sansom, I. D. Kerr, and R. Sankararamakrishnan, Biophys. J. **70**, 693 (1996).
[57] M. Rovere, M. A. Ricci, D. Velatti, and F. Bruni, J. Chem. Phys. **108**, 9859 (1998).
[58] C. Harting, W. Witschel, and E. Spohr, J. Phys. Chem. B **102**, 1241 (1998).
[59] A. Kohlmeyer, C. Harting, and E. Spohr, J. Mol. Liq. **78**, 233 (1998).
[60] E. Spohr, C. Harting, P. Gallo, and M. Rovere, J. Mol. Liq. **80**, 165 (1999).
[61] A. C. Belch and M. Berkowitz, Chem. Phys. Lett. **113**, 278 (1985).
[62] P. Linse, J. Chem. Phys. **90**, 4992 (1989).
[63] P. Linse and B. Halle, Mol. Phys. **67**, 537 (1989).
[64] L. Zhang, H. T. Davis, D. M. Kroll, and H. S. White, J. Phys. Chem. **99**, 2878 (1995).
[65] A. F. Terzis, P. T. Snee, and E. T. Samulski, Chem. Phys. Lett. **264**, 481 (1997).
[66] J. Faeder and B. M. Ladanyi, J. Phys. Chem. B **104**, 1033 (2000).
[67] E. N. Brodskaya, J. C. Eriksson, A. Laaksonen, and A. I. Rusanov, J. Colloid Interface Sci. **180**, 86 (1996).
[68] V. V. Zakharov, E. N. Brodskaya, and A. Laaksonen, J. Chem. Phys. **107**, 10675 (1997).
[69] D. J. Adams, Mol. Phys. **28**, 1241 (1974).
[70] A. Z. Panagiotopoulos, Mol. Phys. **61**, 813 (1987).
[71] A. Z. Panagiotopoulos, Mol. Phys. **62**, 701 (1987).
[72] A. Gonzalez, J. A. White, F. L. Roman, and R. Evans, J. Chem. Phys. **109**, 3637 (1998).
[73] M. Schoen, M. Thommes, and G. H. Findenegg, J. Chem. Phys. **107**, 3262 (1997).
[74] M. Miyahara and K. E. Gubbins, J. Chem. Phys. **106**, 2865 (1997).
[75] M. W. Maddox and K. E. Gubbins, J. Chem. Phys. **107**, 9659 (1997).
[76] W. T. Gozdz, K. E. Gubbins, and A. Z. Panagiotopoulos, Mol. Phys. **84**, 825 (1995).
[77] R. Heintschke, T. Bast, E. Aydt, and M. Kotelyanskii, J. Mol. Model. [Electronic Publication] **2**, 319 (1996).
[78] W. R. Smith and H. L. Vortler, Chem. Phys. Lett. **249**, 470 (1996).
[79] J. C. Shelley and G. N. Patey, J. Chem. Phys. **102**, 7656 (1995).
[80] R. M. Shroll and D. E. Smith, J. Chem. Phys. **110**, 8295 (1999).
[81] S. C. McGrother and K. E. Gubbins, Mol. Phys. **97**, 955 (1999).
[82] A. K. Soper, F. Bruni, and M. A. Ricci, J. Chem. Phys. **109**, 1486 (1998).
[83] F. Scortinio, A. Geiger, and H. E. Stanley, Nature (London) **354**, 218 (1991).
[84] H. E. Stanley, S. V. Buldyrev, and M. Canpolat, Physica A **257**, 213 (1998).
[85] K. Bagchi, S. Balasubramanian, and M. L. Klein, J. Chem. Phys. **107**, 8561 (1997).
[86] F. Franks, in *Water: A Comprehensive Treatise*, edited by F. Franks (Plenum, New York, 1972), Vol. 1, p. 115.